59th ILMENAU SCIENTIFIC COLLOQUIUM
Technische Universität Ilmenau, 11 – 15 September 2017
URN: urn:nbn:de:gbv:ilm1-2017iwk-094:0

INVESTIGATIONS ON THE MECHANICAL RELEVANCE OF PROMINENT VIBRISSA FEATURES FOR SURFACE TEXTURE DETECTION

M. Scharff / J.H. Alencastre / H. Witte / K. Zimmermann / J. Steigenberger / C. Behn

Technische Universität Ilmenau, 98693 Ilmenau, Germany
{moritz.scharff, carsten.behn}@tu-ilmenau.de

Prof. Alencastre is with Pontificial Catholic University of Peru, Lima, Peru

ABSTRACT

The tactile hairs of animals are used as paradigm for artificial tactile sensors. In the case of mystacial vibrissae, the animals can determine the distance to an object, recognize the shape of the object and detect the surface texture of the object. The goal is to design an artificial tactile sensor inspired by the natural paradigm. In the present work, the vibrissa and the follicle-sinus-complex are modeled as a one-sided clamped beam within the limits of the non-linear Euler-Bernoulli beam theory. The theoretical background of the function principle and the effects of typical properties of the natural vibrissa, e.g., a tapered shape and a pre-curvature while operating in surface texture detection are analyzed. The beam-surface contact is described by Coulomb's law of friction. When the beam is in touch with the surface, a quasi-static displacement of the support takes place. As a consequence of the displacement the support reactions are changing. The resulting support reactions are analyzed in parameter studies and beneficial levels of tapering and pre-curvature are identified.

Index Terms— tactile sensor, bio-inspired sensor, animal vibrissa, texture detection, object classification, friction.

1. INTRODUCTION

Autonomous mobile robots rely on various sensory system to fulfill their tasks. Every sensor is constrained by several inherent and external properties and conditions, e.g., the surrounding environment. That holds true for creatures and their sensory system as well. In animal life, tactile hairs are part of the sensory system of several species. For example, mammals have tactile hairs at different locations on their body [1]. There are various types of tactile hairs, e.g., the *carpal* vibrissae at the paws and the *mystacial* vibrissae around the muzzle, see Fig. 1, [2].

Figure 1: Cat with mystacial vibrissae.

Remark 1. *This work focuses on the mystacial vibrissae. In the following, the term vibrissae will be used instead of mystacial vibrissae.*

With their vibrissae animals can detect the distance to an object, recognize the object contour or determine the surface texture, [3], [4]. The typical structure and arrangement of the vibrissae are important for a successful scanning procedure. For the development of an artificial vibrissa-like tactile sensor these properties are important as well and have to be taken into account.

Following, details of the biological paragon are outlined and related mechanical models are discussed. Section 2 introduced the mechanical model, which is used in Section 3 for parameter studies. Finally, Section 4 summarizes the results and gives a short outlook about continuing work.

1.1. State of Art

The vibrissae of rodents, e.g. rats, are arranged in a spatial pattern on each side of the animals muzzle, the so-called mystacial pad, [5]. The shape dimensions of a vibrissa change with the position in this array. While the magnitude of the shape dimensions varies, the basic geometric shape is equal for all vibrissae. The most prominent features are:

- a tapered body, with a decreasing diameter from base to tip,
- the magnitude of dimension of the length is much larger than the magnitude of the diameter,
- along the whole length there is an inherent stressless pre-curvature, [6].

Every single vibrissa is embedded in a *follicle-sinus-complex* (FSC). The FSC itself consists of different types of blood vessels, mechanoreceptors and elastic tissue, [7]. The FSCs are connected to and surrounded by different kinds of muscles and elastic tissue again, [8]. Using these muscles, the animal can move a single vibrissa as well as all vibrissae together. When there is a contact between the vibrissa tip or shaft, the vibrissa transmits the mechanical stimuli to the FSC. In the FSC, the mechanreceptors transduce the mechanical stimuli into a neural potential, [9].

Remark 2. *From the biology's point of view, there is much more information about the scanning process than described. But, for the present work this simplification of the procedure and limitation of information is suitable.*

According to the collected signal, the animals can gather several information, like the distance to an object, the object shape or information about its surface texture. Several hypotheses try to explain how surface texture detection works. The *Resonance Hypothesis* out of the work [10] and the *Kinetic Signature Hypothesis* by [11] are representativly mentioned. The *Kinetic Signature Hypothesis* and the work of [12] relate spike trains of the neural potential with the kinetic behavior of the vibrissa. The information of the surface texture is collected out of sticking and sliding phases of the vibrissa. This scenario is the starting point for the considerations from the mechanical point of view.
There are already different mechanical models of a vibrissa, e.g., for object shape recognition [13], [14], to describe the dynamical behavior [15], to detect flows [16] and for surface texture detection as well. The authors of [17] use a quasi-static finite element model of a beam that is in touch with a rigid body (surface). The beam is assumed as linear elastic, straight and cylindrical. The FSC is modeled as a clamping. So, typical vibrissa features are neglected. The contact between surface and vibrissa is frictionless. The surface texture is modeled as spatial distribution of spaces and groves of macroscopic size. In this scenario, the process of surface texture detection is only a finite number of distance determinations.

Remark 3. *The presented mechanical models for surface texture detection are exemplarily chosen to discuss some important aspects and restrictions. This is not a complete overview of the current state of the art.*

An inherent pre-curved and tapered beam is analyzed in [18]. The beam is modeled as a multi-body system with a quasi-static displacement. The influence of the geometric properties is analyzed for the initial contact with an obstacle. This model is advanced in [19], now considering dynamic properties like effects of inertia and damping. But for both works, there are no further investigations of effects of surface texture. Taking up the idea of the *Resonance Hypothesis*, the authors of [20] study the dynamic behavior of a cylindrical, natural pre-curved beam loaded with a periodic force a the beam tip. It is assumed, that the surface roughness causes the periodic force. But,there is no description between the effect of surface roughness and the periodic force. The model in [21] includes several aspects and details.
The vibrissa is modeled as Euler-Bernoulli beam that respects large deflections in the static case and small vibrations in the dynamic one. The quasi-static displacement of the beam causes large deflections which are superposed with the linear deformation caused by the vibrations. The clamped beam is conically shaped and the contact between beam and surface is a point contact respecting *Coulomb's Law* of friction. The surface itself is characterized by a spatial pattern of spaces and gaps. Only these macroscopic effects are analyzed in context to surface texture properties, friction is included as parasitic effect only.

The work [22] supposes that microscopic surface properties like roughness can be summarized in *Coulomb's Law* of friction [23]. The vibrissa is modeled as a one-sided clamped nonlinear Euler-Bernoulli beam. This model is advanced in [24], [25] and used for the following investigations. All details and restrictions are discussed in Section 2.

1.2. Goal

In the present paper, the effects of tapering and pre-curvature on the measured signals during the surface texture detection are analyzed. The process of surface texture detection is assumed as follows, whereby two perspective have to be considered: the natural one (Fig. 2 I.) and the artificial one (see Fig. 2 II.-III. and section 2).

- First, the animal moves its head forward and the vibrissa gets in touch with the surface and bend, see Fig. 2 I.a)-b). This corresponds to the initial position of the mechanical model, see Fig. 2 II. b). Here, the beam is loaded by an vertical acting force f_y only and its support is located in a fixed vertical distance η to the surface. Out of this state, the animal starts to retract its head.

- The vibrissa tip is sticking to the surface until a certain point, after the sticking phase it will move in any way, see Fig. 2 I.c). In mechanics, this point is reached when the coefficient of static friction μ_0 is reached. A displacement of the support in x-direction yields to a friction force f_x at the tip of the beam, see Fig.2 II.c). When μ_0 is reached the support of the beam is located at the maximal support displacement $x_{0_{max}}$. Figure 2 III.c) shows an exemplary simulation.

Finally, it is possible to determine μ_0 out of the support reactions. The phase after reaching μ_0 is not included in this scenario. Analyzing the described scenario for different levels of tapering and pre-curvature gives information about important design criteria for an artificial tactile sensor.

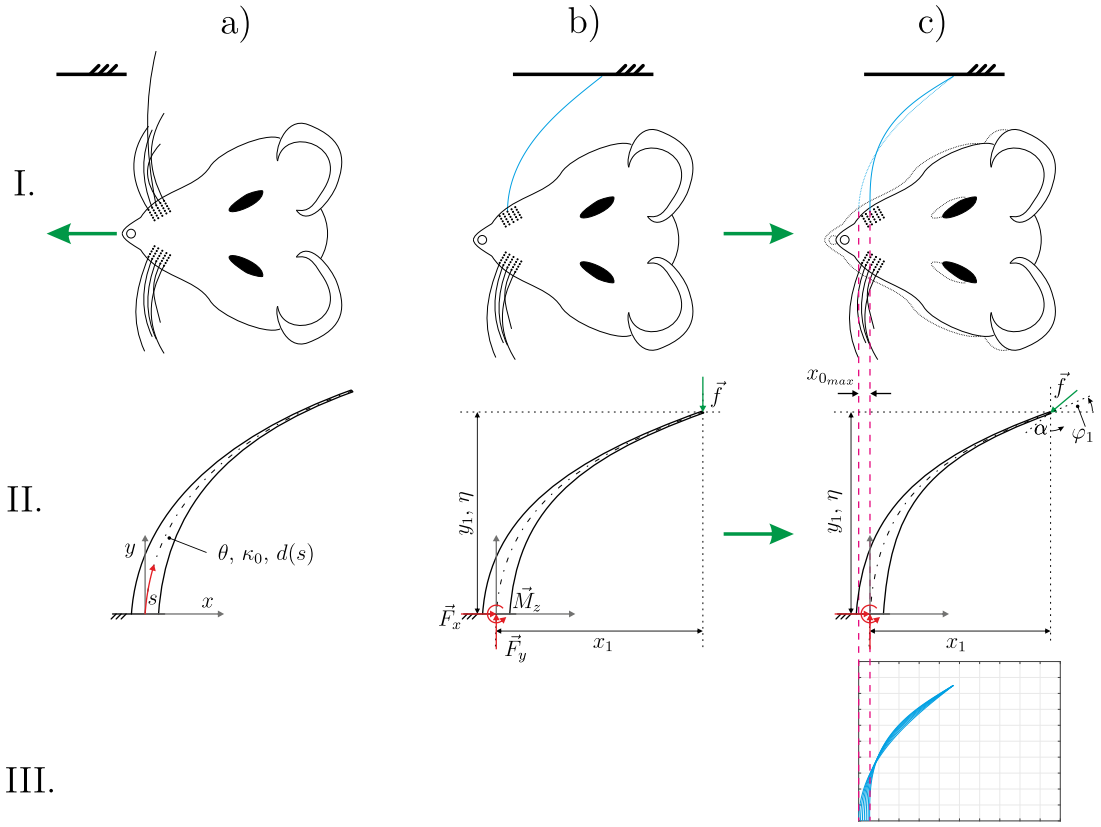

Figure 2: Surface texture scanning procedure: schematic drawing of the biological paragon (I.a)-c)), mechanical modeling (II.a)-c)), numerical simulation of the scanning procedure (III.c)). Column a): state without contact. Column b): state in contact. Column c): scanning.

2. MODELING

Modeling the assumed scenario of surface texture detection the different system components have to be considered. First, the visco-elastic properties of the FSC are neglected. In the mechanical model, it is replaced by an ideal stiff clamping, including the signal processing by evaluating the support reactions. The vibrissa is modeled as Euler-Bernoulli beam considering the following assumptions:

- two dimensional bending in the x-y- plane, respecting large deflections,
- consists of *Hooke's* material,
- a stress free pre-curved beam with a tapered shape.

The contact between vibrissa and surface is modeled as ideal point contact. All the effects resulting of different surface properties, e.g., roughness are summarized in Coulomb's Law of Friction (1):

$$\tan(\alpha) = \frac{|f_x|}{|f_y|} = \mu \leq \mu_0 = \tan(\alpha_0) \tag{1}$$

The beam length L is given with $L = s \cdot [\text{length}]$, with s as arc length:

$$s \in [0, 1]$$

Furthermore, to be independent of the mechanical quantities the model is normalized as follows:

$$\text{units:} \quad [\text{length}] = L\,,\ [\text{force}] = \frac{E\,I_{z0}}{L^2}\,,\ [\text{moment}] = \frac{E\,I_{z0}}{L}$$

with

- L as the length,
- E as the Young's Modulus,
- $I_{z0} = \frac{\pi\, d_0^4}{64}$ as the second moment of area and d_0 as the diameter at the base of the beam.

Remark 4. *For a beam consisting of steel and characterized by the following basic parameters:* $E = 2.10 \cdot 10^5$ *MPa,* $d_0 = 5$ *mm,* $L = 100$ *mm, the dimensionless force* $f = 10.86$ *corresponds to a real force* F*:*

$$F = f \cdot [\textit{force}] = f \cdot \frac{E\,I_{z0}}{L^2} = 7000\,N$$

Since a quasi-static displacement is assumed, the equilibrium state is given with, see Fig. 2 II.c):

$$\left.\begin{array}{lllll} \rightarrow: & F_x + f_x & = 0 & \Longleftrightarrow F_x & = -\,f_x \\ \uparrow: & F_y + f_y & = 0 & \Longleftrightarrow F_y & = -\,f_y \\ \circlearrowleft: & M_z + f_y \cdot x_1 - f_x \cdot y_1 & = 0 & \Longleftrightarrow M_z & = -\,f_y \cdot x_1 + f_x \cdot y_1 \end{array}\right\} \tag{2}$$

while:

$$f_x = \sin(\alpha) \cdot f \qquad ; \qquad f_y = -\cos(\alpha) \cdot f \tag{3}$$

To describe the tapered shape a linear relation between the diameter at the base d_0 of the beam and at the tip d_1 is used:

$$d(s) = -\frac{d_0 - \frac{d_0}{\theta}}{L} s + d_0 \tag{4}$$

with the taper factor θ:

$$\theta := \frac{d_0}{d_1}$$

The stress free pre-curvature κ_0 is constant, whereby A scales its level:

$$\kappa_0 = \frac{A}{8\pi} \tag{5}$$

Combining (2) - (5) yields a nonlinear system of first order differential equations with boundary conditions (6).

$$\left.\begin{aligned} x'(s) &= \cos(\varphi(s)) && ; x(0) &&= x_0; && x(1) = x_1 \\ y'(s) &= \sin(\varphi(s)) && ; y(0) &&= 0; && y(1) = y_1 \\ \varphi'(s) &= \frac{f\theta^4}{(\theta s - \theta - s)^4}\left(\sin(\alpha)(y(s) - y_1) + \cos(\alpha)(x(s) - x_1)\right) - \kappa_0 && ; \varphi(0) &&= \frac{\pi}{2}; && \varphi(1) = \varphi_1 \end{aligned}\right\} \quad (6)$$

As mentioned in Section 1.2, the simulation begins at the initial state and runs until the given μ_0 is reached. So, (6) has to be solved for each increment Δx_0:

$$x_0 = 0 : \Delta x_0 : x_{0_{max}} \quad (7)$$

Remark 5. *For a real sensor μ_0 is unknown and determined out of the measured support reactions. For the simulation this relation is reversed, μ_0 is given as fixed value and the support reactions are evaluated.*

Remark 6. *The assumptions regarding the FSC* (6) *(ideal stiff), the tapering* (4) *(linear) and the pre-curvature κ_0* (5) *(constant) are a dissent from biology. In upcoming simulations, these assumptions have to be improved to match the biological paradigm.*

Applying a *Shooting-Method* in combination with the *Runge-Kutta-Method of 4th order*, the problem is solved.

3. SIMULATION

Figure 3 shows three simulations for different cases which are important for the following parameter studies. In Fig. 3(a) the typical scanning procedure is shown, also see Fig. 2. Here, the base of the beam is moved until μ_0 and $\Delta x_{0_{max}}$ are reached. This is not true for Fig. 3(b) and Fig. 3(c). In Fig. 3(b), $\Delta x_{0_{max}}$ is reached before μ_0 because φ_1 is going to be equal to zero. If φ_1 goes to zero, the beam shape leans to the assumed surface or for negative values of φ_1 the beam shape penetrates the surface. For a real system, the second case is not possible. This effect is caused by the ideal point contact as boundary condition. So, if φ_1 goes to zero the simulation stops. The last special case is shown in Fig. 3(c). The combination of all chosen parameters yields an intensive sticking of the tip and finally a snap off. In this case, there is an suddenly change of φ_1. Considering these effects, the following parameter studies are analyzed.

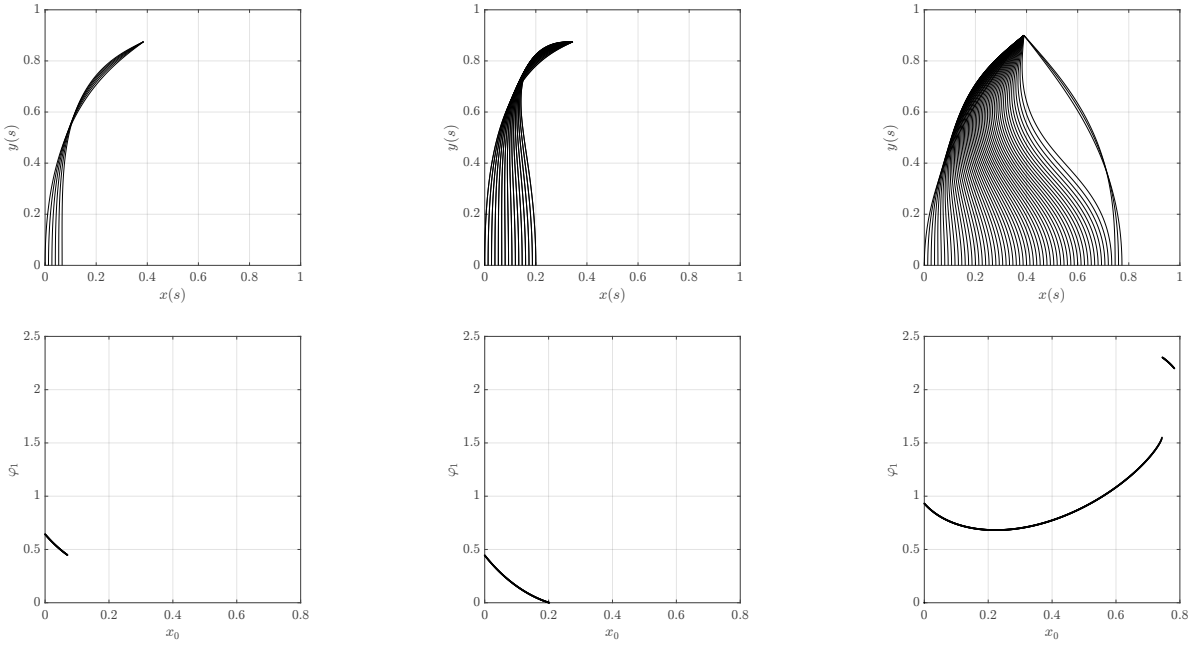

(a) $\eta = 0.875$, $\theta = 2$, $\mu_0 = 0.4$ (b) $\eta = 0.875$, $\theta = 3$, $\mu_0 = 0.5$ (c) $\eta = 0.9$, $\theta = 1$, $\mu_0 = 0.5$

Figure 3: In (a)-(c) three different scenarios are analyzed. The first row shows the elastic shapes while the beam tip is sticking and the second row shows the corresponding φ_1 for every elastica.

The parameter studies are performed for three data sets. All sets are analyzed for a fixed μ_0, Δx_0 and sequences of θ and A. Between these sets, only η varies (see Fig. 2). In Figs. 4-6, the support reactions F_x, F_y and M_z are determined at the maximal clamping displacement $x_{0_{max}}$ and for different θ and A. Furthermore, $x_{0_{max}}$ and φ_1 are evaluated as well.

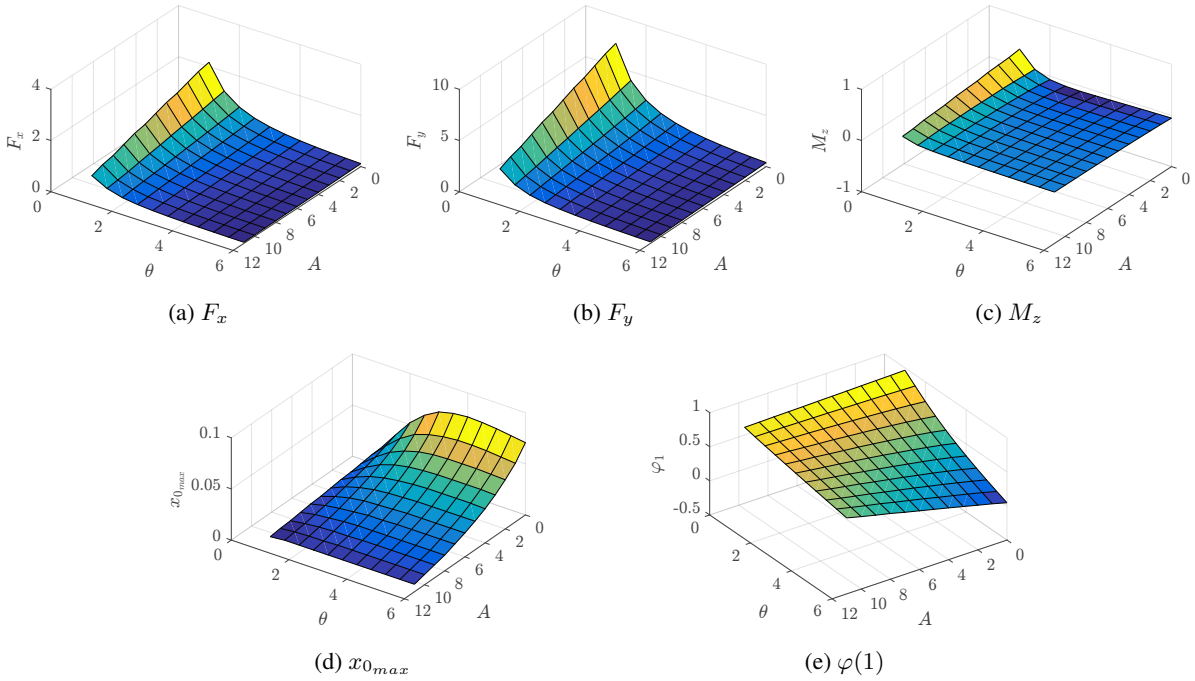

(a) F_x (b) F_y (c) M_z

(d) $x_{0_{max}}$ (e) $\varphi(1)$

Figure 4: Simulations for data set I.: $\eta = 0.925$, $\mu_0 = 0.3$, $\Delta x_0 = \frac{1}{1500}$.

Remark 7. *There are no further simulation for different μ_0 because the obvious relation. A higher μ_0 corresponds to larger support reaction. The fundamental effects of θ and A will not change.*

For the first data set, there are some distinct effects, see Fig. 4:

- for an increasing θ the support reactions are decreasing, this holds true for all levels of A,
- a larger A is related to smaller support reactions for every value of θ,
- at first, $x_{0_{max}}$ gets larger for larger θ but finally it decreases again,
- an increasing A reduces $x_{0_{max}}$ for every θ,
- φ_1 shows the *normal* behavior, see Fig. 3(a), too.

For the second data set there are some changes in comparison to the first one, see Fig. 5. The main findings and statements of the first data set can be confirmed. But for large θ and small A, φ_1 goes to zero. This behavior is explained by Fig. 3(b). For this cases, the simulation ends because of the limits of the algorithm. So, it is not possible to make reliable conclusions for these values of θ and A.

The third data set confirms the principle findings. For increasing θ and A the support reactions are reducing, see Figs. 6(a)-(c). But, Fig. 6(d) shows that there is nearly no displacement of the clamping for large θ and A. This could be caused by two reasons: First, for large θ and small η the value of φ_1 is equal to zero already at small $x_{0_{max}}$. The second reasons is the combination of A, η and μ_0. If A is large and η small the assumed μ_0 is reached at small $x_{0_{max}}$.

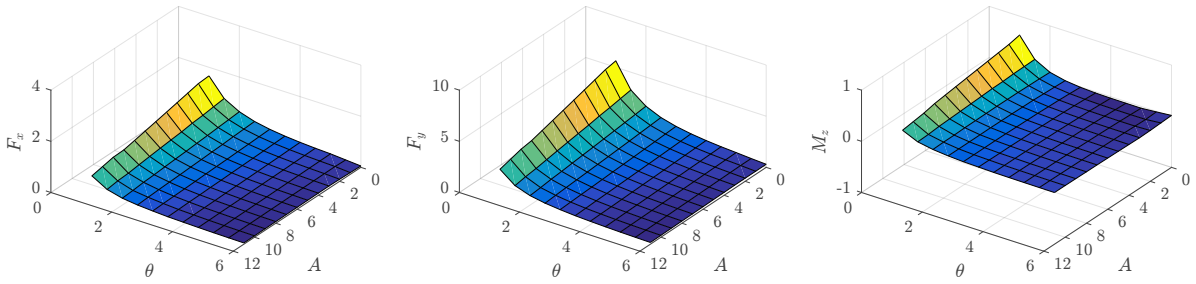

(a) F_x

(b) F_y

(c) M_z

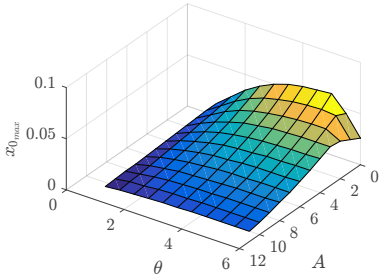

(d) $x_{0_{max}}$

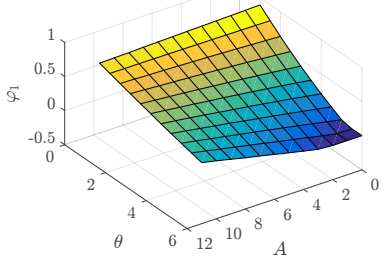

(e) $\varphi(1)$

Figure 5: Simulations for data set II.: $\eta = 0.900$, $\mu_0 = 0.3$, $\Delta x_0 = \frac{1}{1500}$.

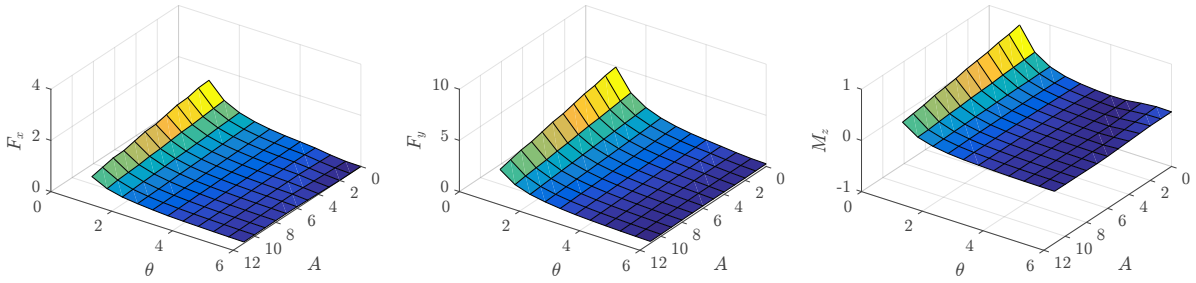

(a) F_x

(b) F_y

(c) M_z

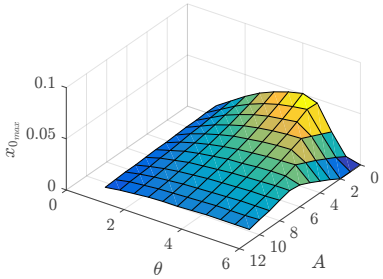

(d) $x_{0_{max}}$

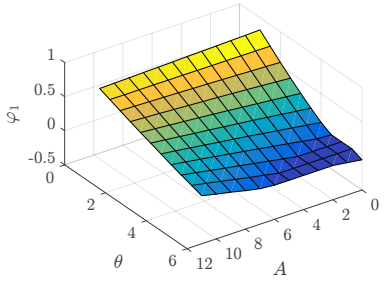

(e) $\varphi(1)$

Figure 6: Simulations for data set III.: $\eta = 0.875$, $\mu_0 = 0.3$, $\Delta x_0 = \frac{1}{1500}$.

4. CONCLUSION

The present work shows the influence of the typical geometric vibrissa properties: tapered shape and stressless pre-curvature on the support reactions. Combinations of different levels of θ, A are analyzed for several η. A larger A yields smaller support reactions for all levels of θ. For small θ the effect is stronger, for larger ones the effect nearly vanishes. At first, a change of θ has a particularly influence on the support reactions, but for large θ there is nearly no change of the support reactions any more.

The results show that it can be useful to design an artificial sensor with a tapered and pre-curved shape if there is a need to influence on the signals at the base. For θ and A, values are identified that make a sensible influence on the signals at the support.
In further steps, the simulation will be advanced, e.g., the contact between beam tip and surface will be enhanced in the way that the beam shape does not penetrate the surface anymore for small η and more features of the natural vibrissa will be implemented. Also, dynamics should be taken into account to verify the results. Next to the theoretical work, there is a need of an experimental proof.

Acknowledgement— This work was supported by the Deutsche Forschungsgemeinschaft, Grant ZI 540-16/2.

5. REFERENCES

[1] T. Helbig, D. Voges, S. Niederschuh, M. Schmidt and H. Witte. The mechanics of carpal vibrissae of rattus norvegicus during substrate contact. In *Proceedings of 58th Ilmenau Scientific Colloquium* (IWK), pages 9, Ilmenau, Germany, 2014, ilmedia.

[2] T. Helbig, D. Voges, S. Niederschuh, M. Schmidt and H. Witte. Characterizing the Substrate Contact of Carpal Vibrissae of Rats during Locomotion. In *Biomimetic and Biohybrid Systems. Living Machines.* pages 399-401, Cham, Switzerland, 2014, Springer.

[3] G.E. Carvell and D.J. Simons. Biometric analyses of vibrissal tactile discrimination in the rat. *Journal of Neuroscience* 10(8): 2638-2648, 1990.

[4] M. Brecht, B. Preilowiski and M.M. Merzenich. Functional architecture of the mystacial vibrissae. *Behavioural Brain Research* 84(1-2): 81-97, 1997.

[5] J. Dörfl. The innervation of the mystacial region of the white mouse: A topographical study. *Journal of Anatomy* 142: 173-184, 1985.

[6] D. Voges, K. Carl, J.G. Klauer, R. Uhlig, C. Schilling, C. Behn and H. Witte Structural Characterization of the Whisker System of the Rat. *IEEE Sensors Journal* 12(2): 332-339, 2012.

[7] F.L. Rice, A. Mance and B.L. Munger. A comparative light microscopic analysis of the sensory innervation of the mystacial pad. I. Innervation of vibrissal follicle-sinus complexes. *Journal of Comparative Neurology* 252(2): 154-174, 1986.

[8] J. Dörfl. The musculature of the mystacial vibrissae of the white mouse. *Journal of Anatomy* 135: 147-154, 1982.

[9] M.E. Diamond and E. Arabzadeh. Whisker sensory system - From receptor to decision. *Progress in Neurobiology* 103: 28-40, 2013.

[10] C.I. Moore and M.L. Andermann. The Vibrissa Resonance Hypothesis. In *Neural plasticity in adult somatic sensory-motor systems. Frontiers in neuroscience.* , pages 21-60, Boca Raton, US, 2005, CRS Press, Taylor & Francis.

[11] E. Arabzadeh, E. Zorzin and M.E. Diamond. Neuronal encoding of texture in the whisker sensory pathway. *PLoS Biology* 3(1): e17, 2005.

[12] J. Wolfe, D.N. Hill, S. Pahlavan, P.J.Drew, D. Kleinfeld. and D.E. Feldman. Texture Coding in the Rat Whisker System: Slip-Stick Versus Differential Resonance. *PLoS Biology* 6(8): e215, 2008.

[13] J.A. Birdwell, J.H. Solomon, M. Thajchayapong, M.A. Taylor, M. Cheely, R.B. Towal, J. Conradt and M.J.Z. Hartmann. Biomechanical Models for Radial Distance Determination by the Rat Vibrissal System. *Journal of Neurophysiology* 98(4): 2439-2455, 2007.

[14] C. Will, J. Steigenberger and C. Behn. Obstacle scanning by technical vibrissae with compilant support. Preprint No. M 15/07, Institute of Mathematics, TU Ilmenau, Germany.

[15] C. Behn, C. Will, and J. Steigenberger. Effects of Boundary Damping on Natural Frequencies in Bending Vibrations of Intelligent Vibrissa Tactile Systems. *International Journal On Advances in Intelligent Systems* 8(3&4): 245-254, 2015.

[16] H. Beem, M. Hildner and M. Triantafyllou. Calibration and validation of a harbor seal whisker-inspired flow sensor. *Smart Materials and Structures* 22(1): 7 pp., 2013.

[17] A. Vaziri, R.A. Jenks, A.R. Boloori and G.B. Stanley. Flexible Probes for Characterizing Surface Topology: From Biology to Technology. *Experimental Mechanics* 47(3): 417-425, 2007.

[18] B.W. Quist and M.J.Z. Hertmann. Mechanical signals at the base of a rat vibrissa: the effect of intrinsic vibrissa curvature and implications for tactile exploration. *Journal of Neurophysiology* 107(9): 2298-1312, 2012.

[19] B.W. Quist, V. Seghete, L.A. Huet, T. Murphey and M.J.Z. Hertmann. Modeling forces and moments at the base of a rat vibrissa during noncontact whisking and whisking against an object. *Journal of Neuroscience* 34(30): 9828-9844, 2014.

[20] T. Volkova, I. Zeidis, H. Witte, M. Schmidt and K. Zimmermann. Analysis of the Vibrissa Parametric Resonance Causing a Signal Amplification during Whisking Behaviour. *Journal of Bionic Engineering* 13(2): 312-323, 2016.

[21] Y. Boubenec, L.N. Claverie, D.E. Schulz, and G. Debrégeas. An amplitude modulation/demodulation scheme for whisker-based texture perception. *Journal of neuroscience* 34(33): 10832-10843, 2014.

[22] J. Steigenberger, C. Behn and C. Will. Mathematical model of vibrissae for surface texture detection. Preprint No. M 15/03, Institute of Mathematics, TU Ilmenau, Germany.

[23] V.L. Popov. *Contact Mechanics and Friction: Physical Principles and Applications.* volume 1, pp. 362, Berlin, Springer, 2010.

[24] M. Scharff, M. Darnieder, J. Steigenberger and C. Behn. Towards the Development of Tactile Sensors for Determination of Static Friction Coefficient to Surfaces. In *Proceedings of Microactuators and Micromechanisms* (MAMM), pages 39-48, Ilmenau, Germany, 2016, Springer.

[25] M. Scharff, C. Behn, J. Steigenberger and J. Alencastre. Towards the Development of Tactile Sensors for Surface Texture Detection. In *The 5th International Conference on Intelligent Systems and Applications* (INTELLI), pages 33-38, Barcelona, Spain, 2016, IARIA.